MATERIALS CHEMISTRY FRONTIERS

CHINESE CHEMICAL SOCIETY

ROYAL SOCIETY OF CHEMISTRY

RESEARCH ARTICLE

View Article Online
View Journal | View Issue

Cite this: *Mater. Chem. Front.*, 2021, **5**, 5371

Hydrogen bond reinforced, transparent polycaprolactone-based degradable polyurethane†

Qianyun Zhong,[a] Xingxing Chen,[a] Yuxuan Yang,[b] Chenhui Cui,[a] Li Ma,[a] Zhen Li,[a] Qiang Zhang,[a] Xiaoming Chen,[c] Yilong Cheng [a] and Yanfeng Zhang *[a]

Received 1st April 2021,
Accepted 5th May 2021

DOI: 10.1039/d1qm00476j

rsc.li/frontiers-materials

Transparent and degradable polyurethane elastomers with high strength and toughness are in demand for various applications, such as tissue engineering and flexible electronics. However, designing specific chemical structures is challenging, and thus fabricating novel elastomers is sometimes unattainable. An effective approach to develop elastomers is through the introduction of sacrificial bonds, *e.g.* hydrogen bonds, to enhance their mechanical properties and toughness, which provide hidden lengths and hierarchical structures for energy dissipation. This study introduced a facile and efficient strategy by employing imidazolidinyl urea (IU) as a multiple hydrogen-bonding motif to fabricate transparent and degradable polyurethane elastomers (PHI) with superior breaking strength and excellent toughness. The resultant breaking strength and toughness reached up to 24.9 MPa and 168.2 MJ m^{-3}, respectively. Additionally, the breaking strength increased to 49.9 MPa after the sample was pre-stretched to 600% strain due to strain-induced crystallization (SIC). Moreover, the PHI film with degradability and good biocompatibility showed potential application in post-operative anti-adhesion.

Introduction

Materials with excellent mechanical properties have broad application prospects in many fields, such as tissue engineering, flexible electronics and displays, *etc.*[1,2] However, it is difficult to combine high mechanical strength, superior toughness, and excellent elasticity in one synthetic polymer because of the complexity and difficulties in molecular design. One of the effective approaches to enhance the strength of elastomers is through physical modification with composite nanofillers; however, compatibility problems and interfacial regulation cannot be avoided.[3–5] On the other hand, biogenic composites including bone,[6] nacre,[6,7] proteins,[8,9] and spider silks[10] reveal excellent strength and high toughness attributed to the presence of sacrificial bonds introducing hidden lengths and complex hierarchical structures,[11–15] including metal–ligand interactions,[16,17] ionic bonds,[18,19] hydrogen bonds,[20–25] *etc.* The breakage of sacrificial bonds prior to the covalent bonds releases hidden lengths and dissipates energy during stretching.[26] After relaxation, the sacrificial bonds can reform to recover their initial mechanical strength and toughness.[11,27–29] Based on this concept, various investigations on sacrificial bonds have been reported in recent years, which established their promising future in polymer materials science.

Inspired by nature, multiple hydrogen bonding motifs were introduced into polymer networks to play the role of sacrificial bonds and provide hierarchical structure.[1,24,30,31] Li *et al.* proposed a biomimetic strategy for strong and tough elastomers constructed by hydrogen bonding interactions with 2-ureido-4[1*H*]-pyrimidione (UPy).[24] However, the introduction of UPy usually required chemical modification of molecules, resulting in cumbersome experimental steps. In our previous work, imidazolidinyl urea (IU) was used as a sacrificial bond agent to endow hydrogels with outstanding mechanical properties.[30,31] In the present study, a facile and effective strategy was proposed to develop transparent and degradable polyurethane elastomers with superior mechanical strength and toughness by incorporating IU as a hydrogen bond agent. Specifically, polycaprolactone (PCL), hexamethylene diisocyanate (HDI), and imidazolidinyl urea (IU) were polymerized to form a linear polymer denoted as PHI, while the multiple hydrogen bonds of IU acted as physical cross-linking agents (Fig. 1a and Fig. S1, ESI†). The resultant transparent and degradable elastomers showed excellent

[a] *School of Chemistry, Xi'an Jiaotong University, Xi'an 710049, China. E-mail: yanfengzhang@mail.xjtu.edu.cn*
[b] *Key Laboratory of Shaanxi Province for Craniofacial Precision Medicine Research, College of Stomatology, Xi'an Jiaotong University, Xi'an 710049, China*
[c] *Micro-and Nanotechnology Research Center, State Key Laboratory for Manufacturing Systems Engineering, Xi'an Jiaotong University, Xi'an, Shaanxi, 710049, China*

† Electronic supplementary information (ESI) available. See DOI: 10.1039/d1qm00476j

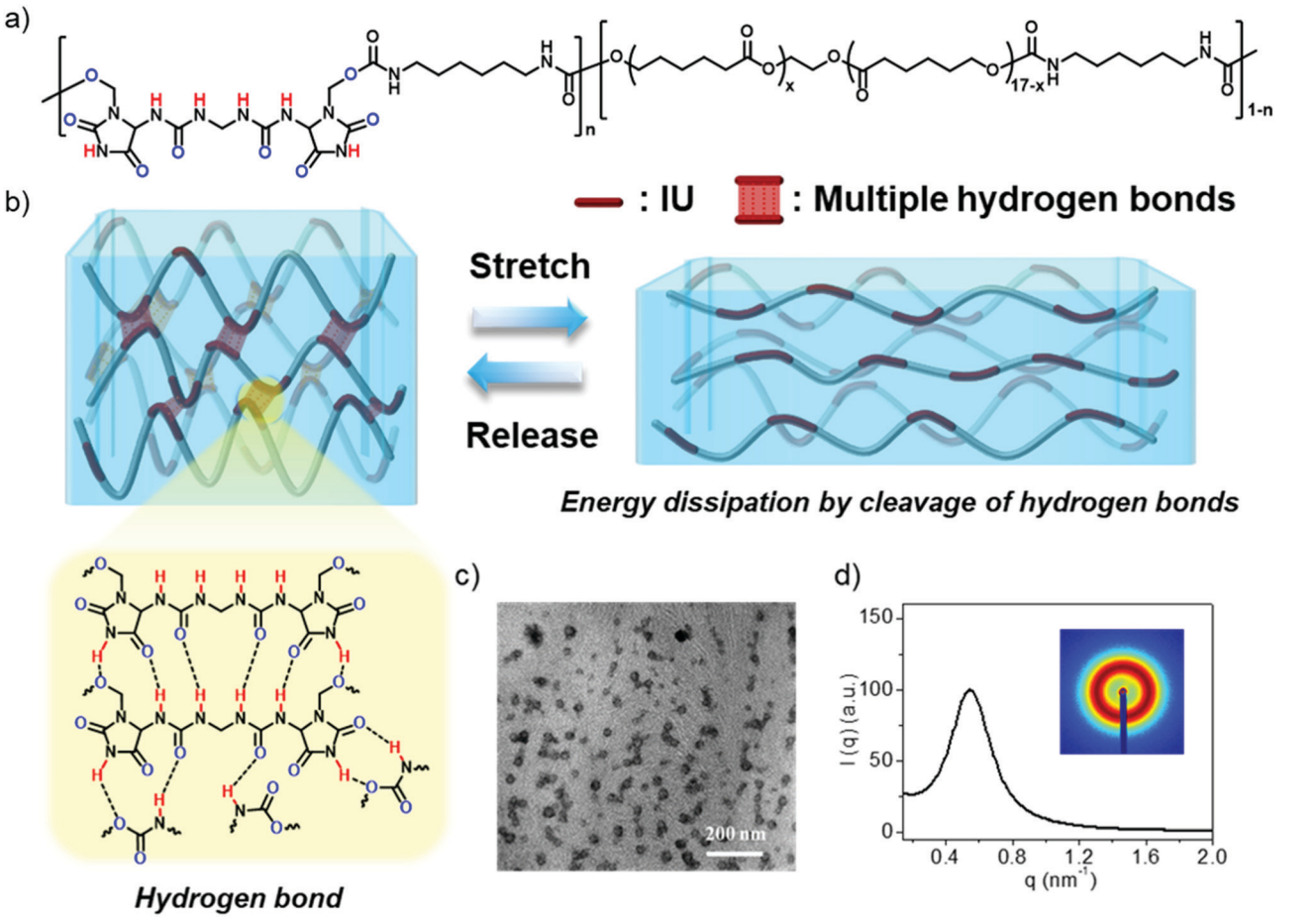

Fig. 1 The schematic preparation procedure of PHI elastomers and characteristics of phase separation. (a) Structure of PHI. (b) Schematic description of the proposed mechanisms for the elastic response under stretching and relaxation. (c) The TEM image of PHI microphase separation. (d) 1D small-angle X-ray scattering (SAXS) profiles of PHI25. Inset: The 2D SAXS image.

mechanical properties, toughness, and acceptable biocompatibility. To explore its potential application, we employed PHI as a physical barrier to investigate the anti-adhesion effect on a mouse abdominal wall injury model.

Experimental

Materials

Hexamethylene diisocyanate (HDI, 97%, Macklin), poly(caprolactone) diol (PCL, M_n = 2000 g mol^{-1}, Acros), imidazolidinyl urea (IU, 98%, Macklin), and dibutyltin dilaurate (DBTDL, 95%, Aladdin) were used as received. *N*,*N*-Dimethylformamide (DMF, 99.5%, Sinorama Technology Co. Ltd) was supplied by Guangdong Sinorama Technology Co. Ltd and used without purification. Experimental animals were purchased from Laboratory Animal Centre, Xi'an Jiaotong University.

Preparation of the PHI film

The synthesis of the thermoplastic polyurethane film was performed using a two-step polymerization process. The synthesis of PHI25 was taken as an example. The prepolymers were prepared in the first step using PCL diol (7.34 mmol), catalyst DBTDL (0.04 g), and HDI (14.68 mmol) in a round bottom flask with 30 g DMF at 85 °C. After 1 h of pre-polymerization, 170 g DMF was added to dilute the system. Afterward, imidazolidinyl urea (7.34 mmol) acting as a chain extender was added to complete the polymerization with rapid stirring at 85 °C for 4 h. The polymer solution was ultrasonically treated and poured into a glass Petri dish (10 × 10 cm). Finally, the samples were dried (60 °C) in a dry air oven for 5 days.

General characterization

^{1}H-NMR (400 MHz) spectra were recorded on a Bruker AVANCE III spectrometer at room temperature using d-DMSO as a solvent. Fourier transform infrared spectroscopy (FTIR) was performed using a Thermo Scientific Nicolet 6700 FTIR spectrometer which was equipped with a diamond ATR crystal at room temperature in the range between 4000 and 400 cm^{-1} with the sampling number of 32. Tandem gel permeation chromatography (GPC) was performed in DMF with 0.1 M LiBr at 40 °C and a flow rate of 1.0 mL min^{-1} on a system equipped with an isocratic pump (Waters 2414). Detection consisted of a DAWN HELEOS

18-angle laser light scattering detector at 658 nm (Wyatt Technology, Santa Barbara, CA) and an Optilab rEX refractive index detector (Wyatt Technology, Santa Barbara, CA). Separations were achieved using size-exclusion columns connected in series (400, 103 and 104 Å phenogel columns, 5 μm, 300 × 7.8 mm, Phenomenex, Torrance, CA). Differential scanning calorimetry (DSC) of the samples was performed on NETZSCH DSC 200PC (NETZSCH Corporation, Germany) apparatus. All the samples were heated from 30 to 100 °C at 20 °C min^{-1} and cooled at 20 °C min^{-1} from 100 to −100 °C under liquid nitrogen (20 mL min^{-1}). To eliminate the thermal history, all data were collected during a second heating run at a scan rate of 10 °C min^{-1} from −100 to 100 °C under a liquid nitrogen atmosphere. Thermogravimetric analysis (TGA) was performed on a NETZSCH TG 209C (NETZSCH Corporation, Germany) using 2–5 mg of sample. Samples were heated under a nitrogen atmosphere at a rate of 20 °C min^{-1} from 30 to 800 °C using an alumina crucible. Transparency tests were performed on a UV-vis spectrophotometer (PE Lambda950, Instrument Analysis Center of Xi'an Jiaotong University). The thickness of all samples ranged from 0.95 to 1.05 nm. The test wavelength was set to 800 to 400 nm, and the reference was air. The mechanical tests were performed on an electronic tensile machine (CMT6503, MTS) with a 5000 N load cell. The samples were cut into dog-bone shapes (sample size 16.0 × 4.0 × 1.0 mm^3) for tests at a rate of 10 mm min^{-1}. In order to quantify the toughness, the value was calculated by eqn (1).

$$\text{Toughness} = \int_{\lambda=0}^{\lambda=\lambda_{\max}} \sigma d\lambda \quad (1)$$

Cyclic tensile deformation processing was carried out using an electronic tensile machine (CMT6503, MTS) at room temperature. Each sample of film was cut into a dog-bone shape (testing measure of 16.0 × 4.0 × 1.0 mm^3). The cyclic tensile deformation was programmed. The specimen was firstly stretched to the required strain at a rate of 10 mm min^{-1}, and then unloaded to reduce the strain until the stress was zero. Once the stress was completely released, the deformation immediately increased again until the target strain was reached. This was cycled until the final number of cycles finished. In addition to the different strain cycles, the PHI samples were cyclically stretched to a strain of 200% for 5 cycles at a rate of 10 mm min^{-1}, and a new tensile deformation was run after relaxation for 2 h. The experiment on a pre-stretched reinforced elastomer was performed on an electronic tensile machine. The samples were pre-stretched to two, four and six times their original length. After deformation, the mechanical tests of the above samples were performed on an electronic tensile machine with a 5000 N load cell at a rate of 10 mm min^{-1}. 2D small angle X-ray scattering (SAXS) measurements were carried out at room temperature on a SAXS instrument (Anton Paar SAXSpoint 2.0) equipped with a Cu/Mo dual microfocal X-ray source and a two-dimensional hybrid photon counting detector (EIGER R 1M) at the Instrumental Analysis Center of Xi'an Jiaotong University. Active area: 77.2 × 79.9 mm, pixel size: 75 × 75 μm. The periodic length L is inversely proportional to the wave vector at the scattering peak (eqn (2)):

$$L = \frac{2\pi}{q} \quad (2)$$

in which q is the q value of the peak in the intensity curves ($I(q) \sim q$).

Transmission electron microscopy (TEM). Thin slices (~50 nm) of the elastomers were prepared by cryotomy. The X-ray diffraction (XRD) measurement was carried out by using an XRD-6100 (Shimadzu XRD-6100, Japan) with Cu Kα radiation. The data were collected between 10 and 80° with a scan speed of 10° min^{-1}.

Puncture resistance test

The film (5 × 5 × 0.88 mm) was clamped between two rectangular sheets of metal. The film can deform freely during the puncture test. A metal needle (the tip diameter was 350 μm) was positioned vertically and moved down to the center of the film in a compression machine with a 50 N sensor and a speed of 50 mm min^{-1}. The puncture energy (E) was calculated by the force–displacement curve integral from eqn (3)

$$E = \int F dl \quad (3)$$

where F is the puncture force at a displacement l.

Solvent resistance at room temperature

The PHI samples were immersed in various solvents of different polarity (5 mL) in glass vials at room temperature. After two days, the samples were dumped, and the residual solvent on the surface was gently wiped with filter paper. The swelling ratio was calculated by eqn (4)

$$\text{Swelling ratio} = \frac{m - m_0}{m_0} \times 100\% \quad (4)$$

where m is the mass of the sample after swelling and m_0 is the mass of the dry sample before swelling.

Degradation experiment

All the samples were cut into long strips (1 × 0.5 cm) using scissors and placed in glass bottle. 5 mL 0.01 M PBS buffer solution and 5 mg lipase were added to the glass bottle, and shaken in a constant temperature shaker at 37 °C. Every 7 days, the sample was washed twice with water, and then washed twice with methanol, dried in a vacuum drying oven at 37 °C, and finally weighed. The weight was calculated by eqn (5)

$$\text{Weight} = \frac{m}{m_0} \times 100\% \quad (5)$$

where m is the mass of the sample after degradation, and m_0 is the mass of the initial sample.

Hemolysis assay *in vitro*

Hemolysis assay *in vitro* was carried out to evaluate the biocompatibility of PHI25 films. Kunming mice were sacrificed to acquire pericardial blood. The blood was collected and firstly gently blended in 10 mL EDTA containing vacutainers. Then the blood was centrifuged at 1500 rpm for 5 min at

4 °C. The total volume of blood was marked and then the serum was removed. After that, the red blood cells (RBC) were re-suspended to the initial volume with freshly prepared 150 mM saline solution. The operation on the blood cells was then repeated more than 2 times to remove remnant serum. After removing the saline solution at the last washing step, red blood cells (400 μL) were suspended with 0.01 M sodium phosphate buffer solution (PBS) to 10 mL to form a 1.11×10^8 mL^{-1} RBC suspension. The PHI25 films (20, 40, and 60 mg mL^{-1}) were added into the RBC suspension as the experiment groups. Saline solution and Triton X-100 (1%) were used as the negative and positive control, respectively. All groups of RBC suspensions were incubated at 37 °C for 1 h. The suspension was collected and centrifuged for 5 minutes at 1500 rpm. 100 μL of supernatant was transferred from each group into a 96 well plate. Finally, the absorbance of the solution was measured with a Multiskan FC microplate reader (Thermo, US) at 541 nm to determine the hemolytic ratio. The hemolysis was calculated by eqn (6)

$$H(100\%) = \frac{A_e - A_c}{A_t} \times 100\% \quad (6)$$

where H is the hemolysis, and A_e, A_c, and A_t are the absorbance at 541 nm for the experiment group, saline solution group, and Triton X-10 group, respectively.

Cytotoxicity assay

The cytotoxicity of the PHI25 film was evaluated through MTT assay. Human normal liver cells (LO2) were seeded in 96-well plates with a density of 1×10^4 per well, and cultured with DMEM media with 10% FBS and a 5% CO_2 atmosphere at 37 °C for 24 hours. The sterilized films were immersed in DMEM culture media without FBS at 37 °C for 24 hours. The supernatant was collected. LO2 cells were incubated with the extraction culture media with 10% FBS for another 1, 2 and 3 days. Subsequently, 20 μL of MTT (5 mg mL^{-1}) was added to each well and incubated at 37 °C for 4 h. After the medium was discarded, 200 μL of DMSO was added to each well to dissolve formazan. Later, 100 μL of the supernatant solution was transferred to a 96-well plate. The absorbance of the solution was measured using a Multiskan FC microplate reader (Thermo, US) at 570 nm. The cell viability was calculated by eqn (7)

$$\text{Cell viability}(100\%) = \frac{A_e - A_b}{A_c - A_b} \times 100\% \quad (7)$$

where A_e, A_b and A_c represent the absorbance of the experiment groups, background groups and blank groups, respectively.

Live/Dead staining

The *in vitro* cytocompatibility of the PHI25 film was further investigated by Live/Dead staining. Live/Dead staining was conducted with human normal liver cells (LO2) seeded into 24-well plates with a density of 2×10^4 per well and cultured in DMEM medium containing 10% FBS under standard cell culture conditions (37 °C and 5% CO_2) for 24 hours. The medium was replaced with fresh medium containing 6.25 mg mL^{-1} PHI25 film. The sample was further cultured at 37 °C, 5% CO_2, for 1, 2 and 3 days. The cell viability was determined by the Live/Dead cytotoxicity tool kit for mammalian cells (Invitrogen®). The green (492 nm) and red (545 nm) fluorescence were observed under a fluorescence microscope (DMi8, Leica, Germany).

In vivo anti-adhesion evaluation of the PHI25 film

All of the animal experiments were approved by the Institutional Animal Care and Use Committee of Xi'an Jiaotong University and in compliance with all regulatory guidelines. The adhesion prevention efficacy of the PHI25 film was evaluated using a model of sidewall defects in mice. Ten Kunming mice (~20 g) were divided into two groups treated with PHI25 film and saline solution, respectively. After anesthesia, the abdominal skin of the mice was depilated and sterilized, and a 1.5 cm incision was made along the midline of the abdomen. Afterward, a 3 × 3 mm abdominal wall defect was created by surgically removing a layer of muscle on the abdominal wall. For the experimental group, a PHI25 film (2 × 2 cm^2) was sutured on the anterior abdominal wall. For comparison, saline solution was also applied to the defect area. Subsequently, the muscle incision was sutured with 6–0 silk thread, and the midline skin incision was closed with 4–0 sutures. At specified time points (1, 2, and 3 weeks), the abdominal cavities were surgically opened to observe and assess the degree of adhesion and the related tissues were collected for further evaluation.

Results and discussion

Different IU contents (25, 33, 38, and 40%) were incorporated as hydrogen bond agents to prepare PHI polymers (Fig. 1a, and Fig. S1 and Table S1, ESI†). IU was a physical crosslinking site in the system to improve the Young's modulus of the material. The chemical structures of the prepared PHI film were characterized by proton nuclear magnetic resonance (^{1}H NMR), Fourier-transform infrared spectroscopy (FTIR), and tandem gel permeation chromatography (GPC), as shown in Fig. S2, S3a, and S4, and Table S1 (ESI†). The hydrogen bonds in the IU structure would dissociate firstly for energy dissipation and the mechanical properties of the bulk material could recover through the re-association of the hydrogen bonds (Fig. 1b). Besides, the microphase separation of the segmented polyurethane (PHI25) was imaged by transmission electron microscopy (TEM) and small angle X-ray scattering (SAXS). The TEM image illustrated the boundary between soft (polycaprolactone; bright zones) and hard domains (multiple H-bonded aggregates; dark spots), as shown in Fig. 1c, which was attributed to the thermodynamic incompatibility between hard and soft segments.[32] The broad peak from the SAXS profiles (q = 0.55 nm^{-1}) corresponding to the periodicity of the phase-separated domains was calculated to be approximately 11.6 nm (Fig. 1d). The amorphous structure was further verified by X-ray diffraction (Fig. S5, ESI†).

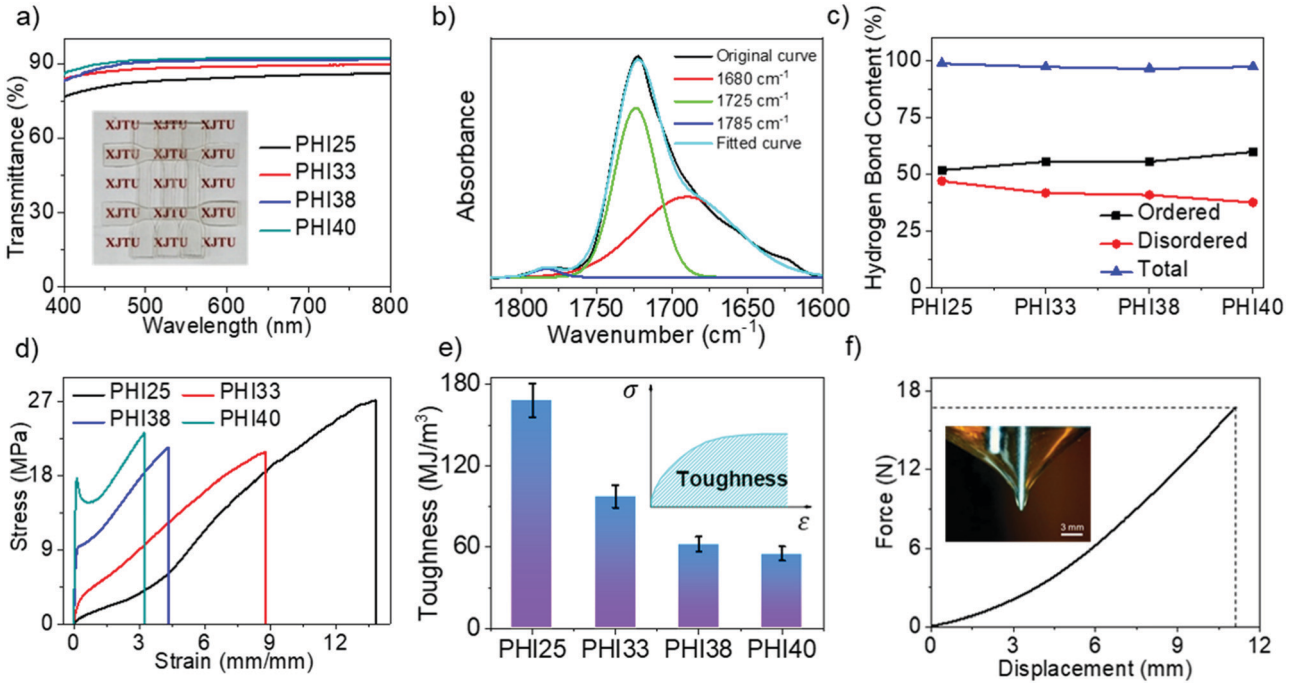

Fig. 2 The characteristics of PHI. (a) UV-vis spectra of PHI films (with a thickness of 0.95 mm) in the visible region. Inset: The photograph of PHI40 films (with a thickness of 0.95 mm) showing that they are transparent and colorless. (b) The FTIR spectrum of PHI25 fitted using Gaussian curves for 1850–1600 cm^{-1}. (c) The change of the FTIR peak intensity of ordered/disordered/total hydrogen bonded C=O for PHI25–PHI40. (d) Stress–strain curves for PHI films stretched at 10 mm min^{-1}. (e) The toughness of the samples. (f) Typical puncture force–displacement curve of PHI25.

Differential scanning calorimetry (DSC) was performed to estimate the glass transition temperature of the PHI polymers. All the polymers showed a T_g of approximately −60 °C (Fig. S6, ESI†). The thermal gravimetric analysis (TGA) data revealed the absence of a decomposition process before 220 °C, which was indicative of excellent thermal stability (Fig. S7, ESI†). A solvent resistance analysis of PHI25 was performed (Fig. S8, ESI†), and the results demonstrated that the PHI25 film had a low swelling ratio in petroleum ether, ether, methanol, and water, while it dramatically swelled in solvents including dichloromethane, chloroform, DMF, and NMP instead of dissolving, suggesting its excellent solvent resistance. Besides, the average transmittance over the entire visible region was above 86% (Fig. 2a), while the PHI0 film was white and opaque (Fig. S9, ESI†). The transparency of the sample gradually increased with increasing IU content, which was attributed to the fact that the hydrogen bonds destroyed the crystallinity of PCL. FTIR spectra analysis was performed to verify the existence of hydrogen bonds, and the results are summarized in Fig. 2b, and Fig. S3b, S3c, and S3d (ESI†). Specifically, the peaks near 1850–1600 cm^{-1} corresponded to the stretching of carbonyl groups, including free carbonyl groups at 1785 cm^{-1}, disordered hydrogen-bonded carbonyl groups at 1725 cm^{-1}, and ordered hydrogen-bonded carbonyl groups at 1680 cm^{-1}. It could be observed from Fig. 2c that the content of hydrogen-bonded carbonyl groups increased with increasing IU content, demonstrating that IU was favorable for the formation of hydrogen bonds.

The mechanical properties of the PHI samples were analyzed by monotonic tensile deformation (Fig. 2d and Table S2, ESI†). The introduction of a small amount of IU could reduce the Young's modulus of the material to a certain extent, which was due to the addition of hydrogen bonds destroying the crystallinity of polycaprolactone. However, the physical crosslinking density of hydrogen bonds increased with the IU content, which eventually led to an increase in the Young's modulus (Fig. S10, ESI†). PHI25, PHI33, and PHI38 exhibited superior fracture strength and ductility similar to rubber, while PHI40 exhibited a yield point and Young's modulus of 17.6 MPa and 293.0 MPa, respectively. With the increase of the IU content, the toughness of the material, which was calculated by the integration of the engineering stress–strain curve, first increased and then decreased (Fig. S11, ESI†). On the one hand, IU provided hydrogen bonds as sacrificial bonds to increase the toughness of the material; on the other hand, IU acted as a physical crosslinking site of hydrogen bonds to improve the mechanical strength. When the content of IU was low, the sacrificial bonds were dominant, and the toughness increased significantly. However, when the content of IU reached a certain value (20%), the physical crosslinking density was too high, which led to the decrease of the toughness. Moreover, the toughness of PHI25 was as high as 168.2 MJ m^{-3} (Fig. 2e), which exceeded most existing degradable materials[33–43] and synthetic fibers,[44] including carbon fibers (25 MJ m^{-3}),[45,46] Kevlar 49 (50 MJ m^{-3}),[45–47] and nylon 6,6 (80 MJ m^{-3}).[45,46] To further verify the remarkable toughness of the PHI25 films, the samples were subjected to a puncture test with a sharp metal needle (Fig. 2f, and Fig. S12 and Video S1, ESI†). The results demonstrated that PHI25 revealed outstanding puncture resistance

with a maximal puncture force and displacement of 16.7 N and 11.1 mm, respectively. Importantly, the puncture energy of PHI25 (72.2 mJ) was larger than that of PHI33 (33.2 mJ, Fig. S13, ESI†) and a commercial tough film (*3M-7605*),[1] highlighting the higher puncture resistance of PHI25. These results were in good agreement with the strain–stress results. Rheology studies showed that the storage modulus and loss modulus of the samples showed a one-step relaxation between 30 and 175 °C (Fig. S14, ESI†), and the increased modulus was attributed to the presence of IU moieties and the resulting physical crosslink density.

Furthermore, cyclic tensile tests were conducted to characterize the mechanical properties of PHI during five successive loading–unloading cycles (Fig. 3a and Fig. S15a–S15c, ESI†). As shown in Fig. S15d (ESI†), the hysteresis area, which is defined as the integration area of the stress–strain curve, increased with deformation. It was hypothesized that the low energy dissipation at low strain was due to the breakage of weak hydrogen bonds in the urethane bonds, while the energy dissipation at higher strain might result from the dissociation of strong multiple hydrogen bonds in IU. In the five consecutive loading–unloading cycles at a strain of 200% (Fig. 3b and Fig. S16, ESI†), the hysteresis energy decreased (Fig. 3c) due to the fact that the residual deformed hydrogen bonds could not recover or re-associate in time. For each cycle, PHI40 had the highest hysteresis area. This was because PHI40 had the highest hydrogen bond content. These results indicated that the dissociation of multiple hydrogen bonds acted as sacrificial bonds, which effectively dissipated the energy during the deformation process. To explore the association–dissociation properties of the hydrogen bonds, PHI40 was first loaded with a strain of 25% and then unloaded for six cycles. After standing for 2 h, a seventh loading–unloading process was performed (Fig. 3d), and it showed a reduced hysteresis loss (1.5 MJ m^{-3}) compared to that of the first cycle (2.6 MJ m^{-3}). The cyclic tensile test curves of PHI25, PHI33, and PHI38 with similar mechanical behaviors in continuous cycles after a delay of 2 h are summarized in Fig. S17 (ESI†). Hydrogen bonds acting as sacrificial bonds would break during the stretching process, which led to great energy dissipation. In a relaxed state, the hydrogen bonds in the polymer reconstituted to a certain extent, and the hysteresis energy recovered.

Previous reports stated that a crystalline microstructure dispersed in an amorphous polymer matrix can greatly enhance its mechanical properties.[11,48–50] PHI25 was pre-stretched to two, four, and six times its original length to induce the arrangement of microstructure prior to mechanical testing. After deformation, the mechanical properties of the above samples were analyzed by a tensile test, and the results are shown in Fig. 3e and summarized in Table S3 (ESI†). In particular, the Young's modulus and breaking strength increased with the degree of deformation, whereas the breaking strain and toughness decreased. Importantly, the breaking strength of PHI25 was 49.9 MPa with a pre-stretched elongation

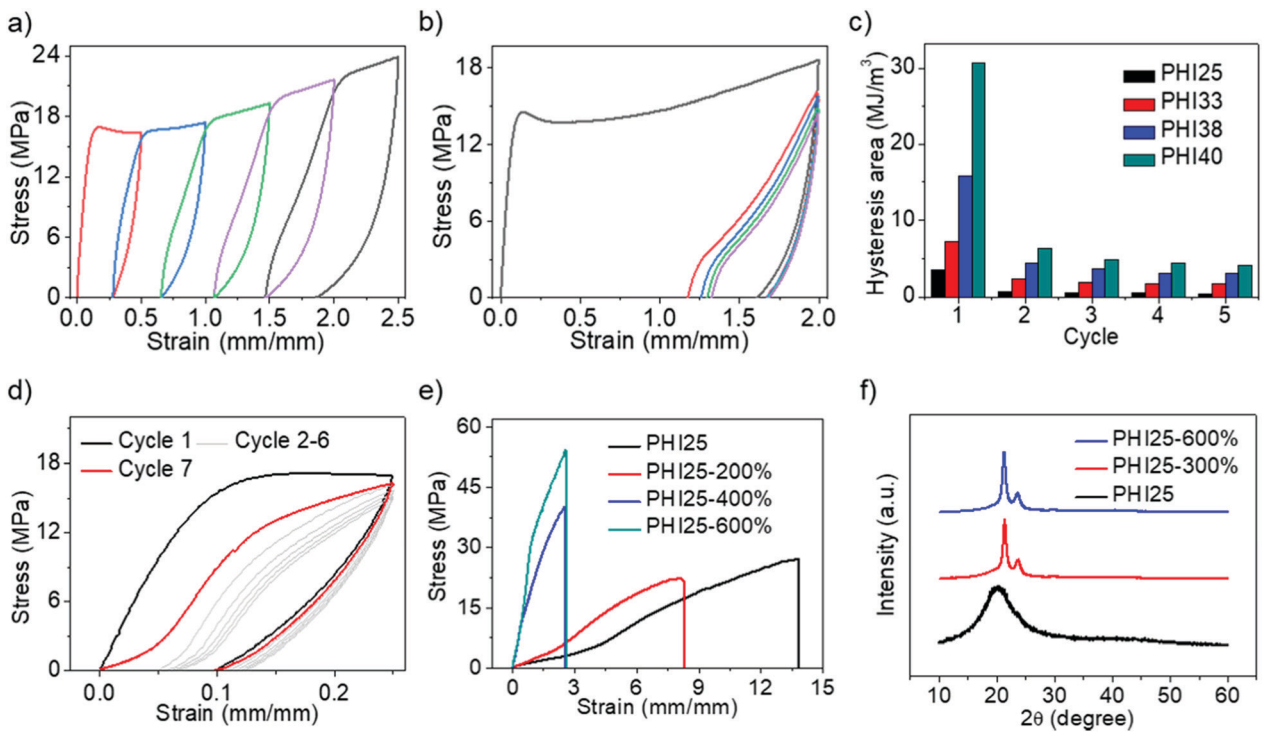

Fig. 3 Step-cycle tensile deformation and stretching as a processing method to improve the mechanical properties. (a) Loading–unloading curves of PHI40 under different strains. (b) Five successive loading–unloading cycles of PHI40 at a strain of 200%. (c) Dissipated energy during five successive loading–unloading processes at a strain of 200% in every cycle. (d) Cyclic tensile test curves in successive cycles of PHI40. The loading–unloading cycle 7 was delayed for 2 h after cycle 6. (e) Stress–strain curves for PHI25 pre-stretched to different deformations varying from 200 to 600%. (f) XRD curves for PHI25 films at different deformations.

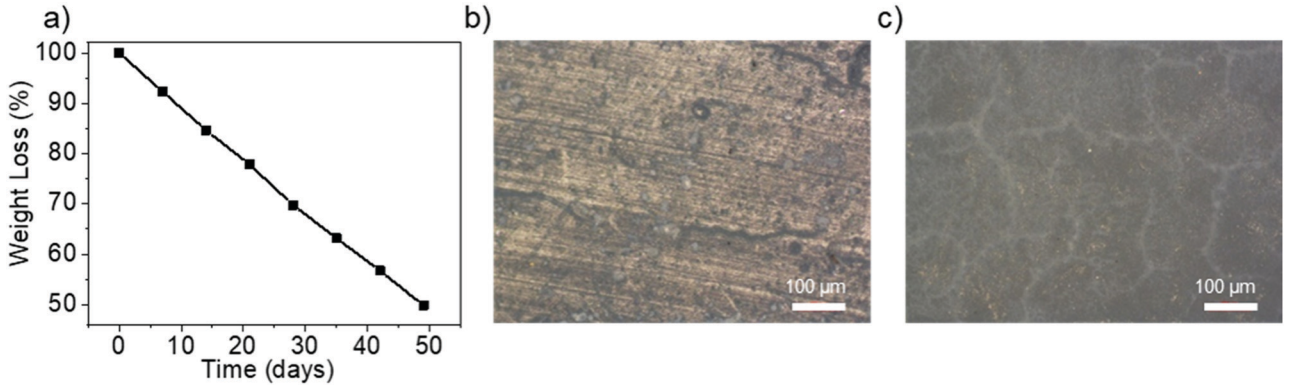

Fig. 4 The degradation performance of PHI. (a) Mass loss of PHI25 as a function of degradation time. (b and c) Optical microscope images of PHI25 at different weight loss. b: 0% weight loss; c: 50% weight loss.

of 600%, which was twice that of the as-synthesized sample (24.9 MPa) and stemmed from the strain-induced crystallization of the PCL chain. Besides, PHI33, PHI38, and PHI40 showed similar mechanical behavior due to the crystallized PCL (Fig. S18 and Table S4, ESI†). This hypothesis was verified by X-ray diffraction (XRD) analysis under different pre-stretched deformation (Fig. 3f and Fig. S19, ESI†), where the peak at 23.6 degrees increased with deformation. On the other hand, the dissociation and re-association of hydrogen bonds might change the topological rearrangement of the polymer and limit the mobility of the PCL chain, facilitating the formation of a new nanostructure.[48,51]

The enzymatic hydrolysis process of PCL-based polyurethane mainly relies on the hydrolysis of carbamate bonds. Firstly, lipase attacks the ester bonds and hydrolyzes the polyurethane. At the same time, it hydrolyzes the amide bonds, destroys the polyurethane polymer chain, and generates low molecular weight compounds. Afterward, the polyurethane fragment is further broken to complete the degradation process.[52] Fig. 4a and Fig S20 (ESI†) show the mass loss curve of the PHI films with time at 37 °C under the action of 0.01 M PBS buffer and lipase. The degradation rate of sample PHI25 in four samples was fast due to the high content of the PCL segment in the networks.

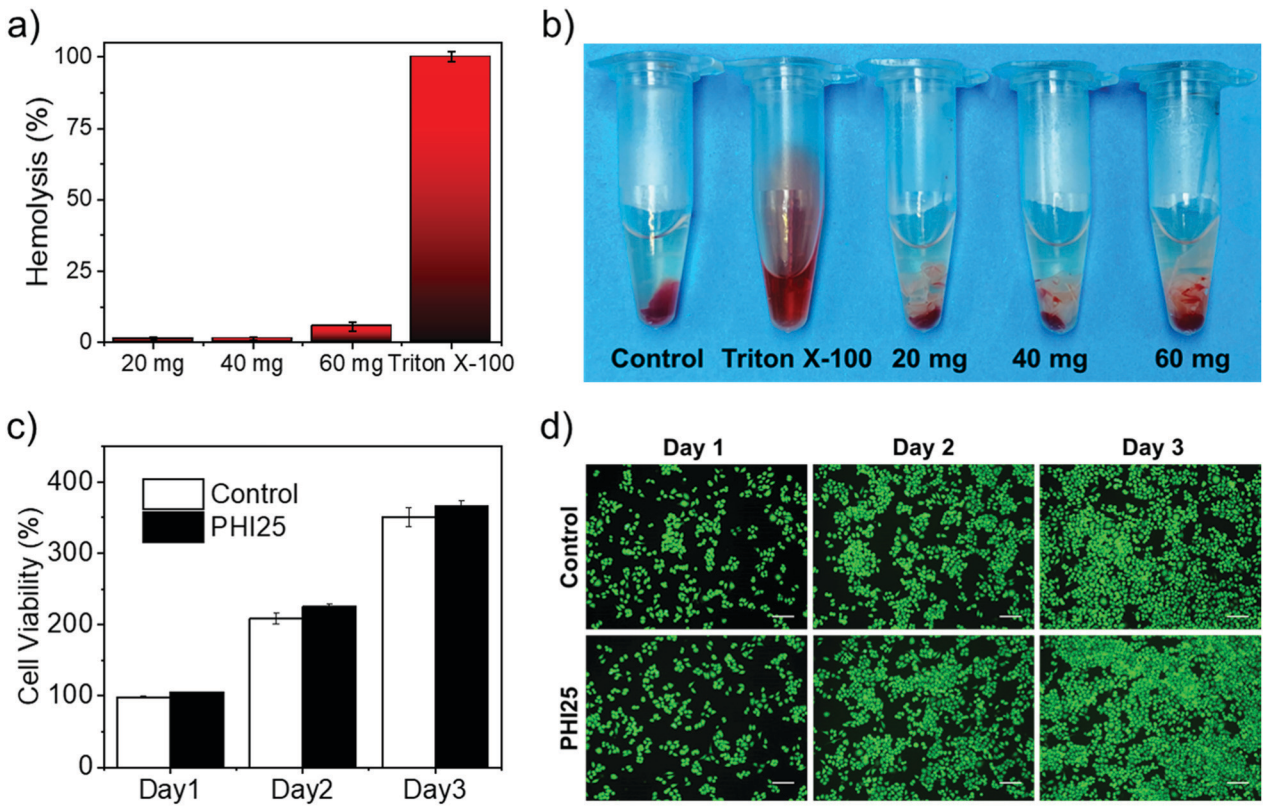

Fig. 5 *In vitro* experiments of PHI25 films. (a) Hemolytic percentage of PHI25 films. (b) Photo from hemolytic activity experiments of PHI25 films. (c) Cell viability treated with PHI25 films by assay. (d) Live/Dead assay of LO2 cells treated with PHI25 films. The TCP wad served as a control. Scale bar: 100 μm.

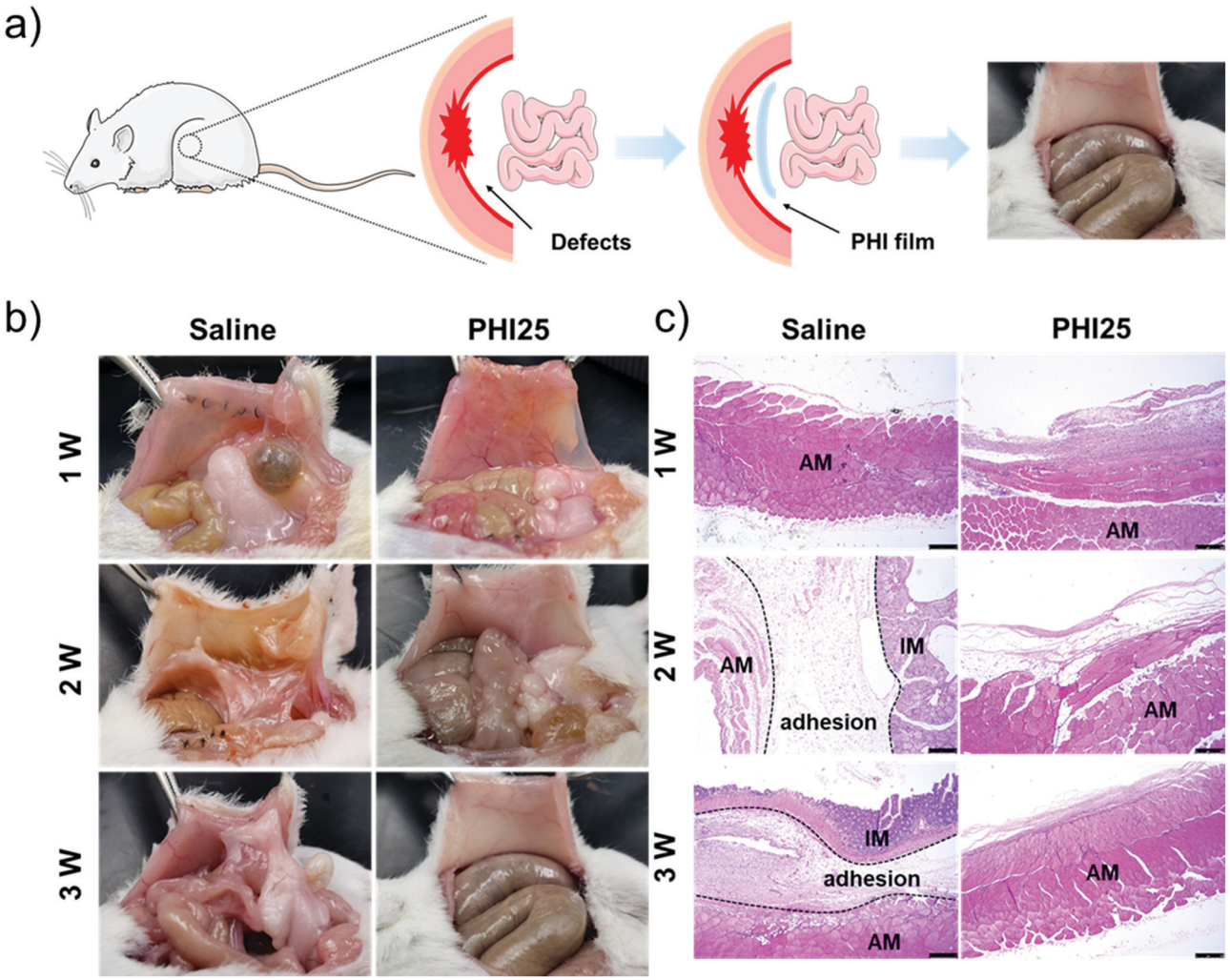

Fig. 6 *In vivo* experiments of PHI25 films. (a) Illustration of the abdominal defect model in mice by using PHI25 as a physical barrier. (b) Gross observation of the anti-adhesive efficacy treated with saline and PHI25 films. (c) Histological examination of the injured sites after surgery. AW: abdominal wall; IM: intestinal mucosa.

Moreover, PHI25 showed a linear degradation trend. After degradation for 49 days, the mass loss of PHI25 reached 50%. Optical micrographs of PHI25 at different weight losses before and after degradation are shown in Fig. 4b and c. The surface of PHI25 became rougher and cracks were formed on the surface with increasing mass loss.

To explore the potential application of PHI in biomedical applications, we first evaluated the *in vitro* blood and cell compatibility. As shown in Fig. 5a, PHI25 showed negligible hemolysis with a concentration of 20, 40, and 60 mg mL^{-1}. Compared with the positive control group (Triton X-100), the supernatant of the experimental groups and the normal saline groups was light yellow, indicating that the PHI25 films showed good blood compatibility (Fig. 5b). Moreover, the cytocompatibility of the PHI25 films was evaluated by MTT assay and Live/Dead staining. Human normal liver cells (LO2) in the experimental groups had a similar proliferation trend to a tissue culture plate (TCP), and the cells proliferated 2.3 and 3.7 times after 2 and 3 days, respectively (Fig. 5c). As displayed in Fig. 5d, little red fluorescence (dead cells) was found in the PHI25 film treatment groups during the whole cultivation process, indicating good cytocompatibility of PHI25.

Peritoneal adhesion is proliferative fibrin bands formed between the damaged abdominal wall and adjacent normal organs after an operation.[53] It is a common complication after a peritoneal operation.[54] The physical barrier strategy is one of the effective methods to inhibit postoperative adhesion.[30,55,56] In view of the excellent mechanical properties, toughness, degradability and good biocompatibility of PHI25, it was expected to have potential application in post-operative anti-adhesion. A mouse model of abdominal injury was established to evaluate the anti-adhesion behavior of PHI25 films (Fig. 6a). Mice only treated with saline were used as a control. PHI25 films were implanted between the damaged abdominal wall and cecum. In the saline treatment groups, adhesion appeared one week later, and, with the extension of time, the adhesion became more and more serious (Fig. 6b). Compared with the saline treatment groups, the PHI25 films did not cause any

adhesion within three weeks, indicating a satisfactory anti-adhesion effect. In particular, no abdominal wall defect was observed in the PHI25 film treatment groups, indicating that PHI25 films would not affect the normal recovery of the wound. The inflammatory response in the surgical site was detected by H&E staining. As depicted in Fig. 6c, two weeks later, neutrophil infiltration and a large amount of fibrous tissue were observed in the saline treatment groups, indicating the existence of serious abdominal adhesion. On the contrary, no adhesion or obvious inflammation were found in the PHI25 film treatment groups during the whole treatment process, indicating that PHI25 films could effectively prevent the occurrence of adhesion.

Conclusions

In summary, a simple and efficient molecular design was proposed to prepare a transparent polyurethane with excellent properties by incorporating IU motifs in the skeleton of the polymer. The hydrogen bonds served as physical crosslinking points and sacrificial bonds, which endowed the elastomer with high mechanical properties and remarkable toughness (168.2 MJ m^{-3}). The dynamic association–dissociation mechanism of hydrogen bonds contributed to the recovery of the mechanical properties. Moreover, the strain-induced crystallization behavior of the soft PCL segment during stretching was verified by XRD and was determined to have a positive effect on improving the mechanical properties. In addition, PHI showed good blood and cell biocompatibility, and could act as physical barriers to prevent adhesion in a mouse model of abdominal injury. Therefore, PHI may show vast potential in biomedical fields.

Conflicts of interest

There are no conflicts to declare.

Acknowledgements

The authors gratefully acknowledge the financial support from the National Natural Science Foundation of China (NSFC 51873170, 11732012), the National Key R&D Program of China (2019YFA0706801), the Key Laboratory Construction Program of Xi'an Science and Technology Bureau (201805056ZD7CG40), the "Young Talent Support Plan" of Xi'an Jiaotong University, the One Hundred Talents Program of Shaanxi Province and The Shaanxi Key Industry Innovation Chain Project (No. 2019ZDLGY02-02). The authors gratefully acknowledge Junjie Zhang at School of Chemistry of Xi'an Jiaotong University for his assistance with DSC, TGA, mechanical property, NMR, FTIR, and UV-vis analysis.

Notes and references

1 X. Chen, Q. Zhong, C. Cui, L. Ma, S. Liu, Q. Zhang, Y. Wu, L. An, Y. Cheng, S. Ye, X. Chen, Z. Dong, Q. Chen and Y. Zhang, Extremely Tough, Puncture-Resistant, Transparent, and Photoluminescent Polyurethane Elastomers for Crack Self-Diagnose and Healing Tracking, *ACS Appl. Mater. Interfaces*, 2020, **12**, 30847.
2 E. R. P. Pinto, H. S. Barud, R. R. Silva, M. Palmieri, W. L. Polito, V. L. Calil, M. Cremona, S. J. L. Ribeiro and Y. Messaddeq, Transparent composites prepared from bacterial cellulose and castor oil based polyurethane as substrates for flexible OLEDs, *J. Mater. Chem. C*, 2015, **3**, 11581.
3 Z. Tang, L. Zhang, W. Feng, B. Guo, F. Liu and D. Jia, Rational Design of Graphene Surface Chemistry for High-Performance Rubber/Graphene Composites, *Macromolecules*, 2014, **47**, 8663.
4 N. Bitinis, M. Hernandez, R. Verdejo, J. M. Kenny and M. A. Lopez-Manchado, Recent Advances in Clay/Polymer Nanocomposites, *Adv. Mater.*, 2011, **23**, 5229.
5 H. Wei, Y. Yang, X. Huang, Y. Zhu, H. Wang, G. Huang and J. Wu, Transparent, robust, water-resistant and high-barrier self-healing elastomers reinforced with dynamic supramolecular nanosheets with switchable interfacial connections, *J. Mater. Chem. A*, 2020, **8**, 9013.
6 H. D. Espinosa, J. E. Rim, F. Barthelat and M. J. Buehler, Merger of structure and material in nacre and bone – Perspectives on de novo biomimetic materials, *Prog. Mater. Sci.*, 2009, **54**, 1059.
7 A. Walther, I. Bjurhager, J.-M. Malho, J. Ruokolainen, L. Berglund and O. Ikkala, Supramolecular Control of Stiffness and Strength in Lightweight High-Performance Nacre-Mimetic Paper with Fire-Shielding Properties, *Angew. Chem., Int. Ed.*, 2010, **49**, 6448.
8 A. M. Kushner, J. D. Vossler, G. A. Williams and Z. Guan, A Biomimetic Modular Polymer with Tough and Adaptive Properties, *J. Am. Chem. Soc.*, 2009, **131**, 8766.
9 A. M. Kushner, V. Gabuchian, E. G. Johnson and Z. Guan, Biomimetic Design of Reversibly Unfolding Cross-Linker to Enhance Mechanical Properties of 3D Network Polymers, *J. Am. Chem. Soc.*, 2007, **129**, 14110.
10 N. Becker, E. Oroudjev, S. Mutz, J. P. Cleveland, P. K. Hansma, C. Y. Hayashi, D. E. Makarov and H. G. Hansma, Molecular nanosprings in spider capture-silk threads, *Nat. Mater.*, 2003, **2**, 278.
11 E. Degtyar, M. J. Harrington, Y. Politi and P. Fratzl, The Mechanical Role of Metal Ions in Biogenic Protein-Based Materials, *Angew. Chem., Int. Ed.*, 2014, **53**, 12026.
12 J. Currey, Sacrificial bonds heal bone, *Nature*, 2001, **414**, 699.
13 M. A. Meyers, P.-Y. Chen, A. Y.-M. Lin and Y. Seki, Biological materials: Structure and mechanical properties, *Prog. Mater. Sci.*, 2008, **53**, 1.
14 G. Mayer, Rigid Biological Systems as Models for Synthetic Composites, *Science*, 2005, **310**, 1144.
15 X. Zhou, B. Guo, L. Zhang and G.-H. Hu, Progress in bio-inspired sacrificial bonds in artificial polymeric materials, *Chem. Soc. Rev.*, 2017, **46**, 6301.
16 J. Min, H. Zhang, T. Stubhan, Y. N. Luponosov, M. Kraft, S. A. Ponomarenko, T. Ameri, U. Scherf and C. J. Brabec, A combination of Al-doped ZnO and a conjugated polyelectrolyte interlayer for small molecule solution-processed

solar cells with an inverted structure, *J. Mater. Chem. A*, 2013, **1**, 11306.
17 C.-H. Li, C. Wang, C. Keplinger, J.-L. Zuo, L. Jin, Y. Sun, P. Zheng, Y. Cao, F. Lissel, C. Linder, X.-Z. You and Z. Bao, A highly stretchable autonomous self-healing elastomer, *Nat. Chem.*, 2016, **8**, 618.
18 L. Zhang, L. R. Kucera, S. Ummadisetty, J. R. Nykaza, Y. A. Elabd, R. F. Storey, K. A. Cavicchi and R. A. Weiss, Supramolecular Multiblock Polystyrene–Polyisobutylene Copolymers via Ionic Interactions, *Macromolecules*, 2014, **47**, 4387.
19 T. L. Sun, T. Kurokawa, S. Kuroda, A. B. Ihsan, T. Akasaki, K. Sato, M. A. Haque, T. Nakajima and J. P. Gong, Physical hydrogels composed of polyampholytes demonstrate high toughness and viscoelasticity, *Nat. Mater.*, 2013, **12**, 932.
20 J. Wu, L.-H. Cai and D. A. Weitz, Tough Self-Healing Elastomers by Molecular Enforced Integration of Covalent and Reversible Networks, *Adv. Mater.*, 2017, **29**, 1702616.
21 X. Hu, J. Zhou, W. F. M. Daniel, M. Vatankhah-Varnoosfaderani, A. V. Dobrynin and S. S. Sheiko, Dynamics of Dual Networks: Strain Rate and Temperature Effects in Hydrogels with Reversible H-Bonds, *Macromolecules*, 2017, **50**, 652.
22 J. A. Neal, D. Mozhdehi and Z. Guan, Enhancing Mechanical Performance of a Covalent Self-Healing Material by Sacrificial Noncovalent Bonds, *J. Am. Chem. Soc.*, 2015, **137**, 4846.
23 D. Zhao, G. Chen, H. Yao and Y. Song, Reinforcement of polysiloxane/silica elastomer composite by introduction of sacrificial bonds, *J. Appl. Polym. Sci.*, 2018, **135**, 46129.
24 Y. Song, Y. Liu, T. Qi and G. L. Li, Towards Dynamic but Supertough Healable Polymers through Biomimetic Hierarchical Hydrogen-Bonding Interactions, *Angew. Chem., Int. Ed.*, 2018, **57**, 13838.
25 B. J. Gold, C. H. Hövelmann, C. Weiss, A. Radulescu, J. Allgaier, W. Pyckhout-Hintzen, A. Wischnewski and D. Richter, Sacrificial bonds enhance toughness of dual polybutadiene networks, *Polymer*, 2016, **87**, 123.
26 H. Li, A. F. Oberhauser, S. B. Fowler, J. Clarke and J. M. Fernandez, Atomic force microscopy reveals the mechanical design of a modular protein, *Proc. Natl. Acad. Sci. U. S. A.*, 2000, **97**, 6527.
27 G. E. Fantner, T. Hassenkam, J. H. Kindt, J. C. Weaver, H. Birkedal, L. Pechenik, J. A. Cutroni, G. A. G. Cidade, G. D. Stucky, D. E. Morse and P. K. Hansma, Sacrificial bonds and hidden length dissipate energy as mineralized fibrils separate during bone fracture, *Nat. Mater.*, 2005, **4**, 612.
28 B. L. Smith, T. E. Schäffer, M. Viani, J. B. Thompson, N. A. Frederick, J. Kindt, A. Belcher, G. D. Stucky, D. E. Morse and P. K. Hansma, Molecular mechanistic origin of the toughness of natural adhesives, fibres and composites, *Nature*, 1999, **399**, 761.
29 H. Wang, H. Liu, Z. Cao, W. Li, X. Huang, Y. Zhu, F. Ling, H. Xu, Q. Wu, Y. Peng, B. Yang, R. Zhang, O. Kessler, G. Huang and J. Wu, Room-temperature autonomous self-healing glassy polymers with hyperbranched structure, *Proc. Natl. Acad. Sci. U. S. A.*, 2020, **117**, 11299.
30 Y. Yang, X. Zhao, J. Yu, X. Chen, X. Chen, C. Cui, J. Zhang, Q. Zhang, Y. Zhang, S. Wang and Y. Cheng, H-Bonding Supramolecular Hydrogels with Promising Mechanical Strength and Shape Memory Properties for Postoperative Antiadhesion Application, *ACS Appl. Mater. Interfaces*, 2020, **12**, 34161.
31 J. Yu, X. Chen, Y. Yang, X. Zhao, X. Chen, T. Jing, Y. Zhou, J. Xu, Y. Zhang and Y. Cheng, Construction of supramolecular hydrogels using imidazolidinyl urea as hydrogen bonding reinforced factor, *J. Mater. Chem. B*, 2020, **8**, 3058.
32 S. L. Cooper and A. V. Tobolsky, Properties of linear elastomeric polyurethanes, *J. Appl. Polym. Sci.*, 1966, **10**, 1837.
33 Y. Sun, Z. Liu, F. Chen, M. Xu, J. Zhang and W. Li, Hierarchical Cross-Linked Poly(caprolactone-*co*-urethane) toward Connective Tissue-like Properties and Multifunctional Integration, *Chem. Mater.*, 2019, **31**, 9295.
34 A. Watts and M. A. Hillmyer, Aliphatic Polyester Thermoplastic Elastomers Containing Hydrogen-Bonding Ureidopyrimidinone Endgroups, *Biomacromolecules*, 2019, **20**, 2598.
35 T. T. Truong, S. H. Thai, H. T. Nguyen, D. T. T. Phung, L. T. Nguyen, H. Q. Pham and L.-T. T. Nguyen, Tailoring the Hard–Soft Interface with Dynamic Diels–Alder Linkages in Polyurethanes: Toward Superior Mechanical Properties and Healability at Mild Temperature, *Chem. Mater.*, 2019, **31**, 2347.
36 B. J. Green, K. S. Worthington, J. R. Thompson, S. J. Bunn, M. Rethwisch, E. E. Kaalberg, C. Jiao, L. A. Wiley, R. F. Mullins, E. M. Stone, E. H. Sohn, B. A. Tucker and C. A. Guymon, Effect of Molecular Weight and Functionality on Acrylated Poly(caprolactone) for Stereolithography and Biomedical Applications, *Biomacromolecules*, 2018, **19**, 3682.
37 X. Kuang, K. Chen, C. K. Dunn, J. Wu, V. C. F. Li and H. J. Qi, 3D Printing of Highly Stretchable, Shape-Memory, and Self-Healing Elastomer toward Novel 4D Printing, *ACS Appl. Mater. Interfaces*, 2018, **10**, 7381.
38 A. Saralegi, S. C. M. Fernandes, A. Alonso-Varona, T. Palomares, E. J. Foster, C. Weder, A. Eceiza and M. A. Corcuera, Shape-Memory Bionanocomposites Based on Chitin Nanocrystals and Thermoplastic Polyurethane with a Highly Crystalline Soft Segment, *Biomacromolecules*, 2013, **14**, 4475.
39 D. Wan, Q. Jiang, Y. Song, J. Pan, T. Qi and G. L. Li, Biomimetic Tough Self-Healing Polymers Enhanced by Crystallization Nanostructures, *ACS Appl. Polym. Mater.*, 2020, **2**, 879.
40 G. S. Sulley, G. L. Gregory, T. T. D. Chen, L. Peña Carrodeguas, G. Trott, A. Santmarti, K.-Y. Lee, N. J. Terrill and C. K. Williams, Switchable Catalysis Improves the Properties of CO_2-Derived Polymers: Poly(cyclohexene carbonate-*b*-ε-decalactone-*b*-cyclohexene carbonate) Adhesives, Elastomers, and Toughened Plastics, *J. Am. Chem. Soc.*, 2020, **142**, 4367.
41 T. Ghosh and N. Karak, Tough interpenetrating polymer network of silicone containing polyurethane and polystyrene with self-healing, shape memory and self-cleaning attributes, *RSC Adv.*, 2018, **8**, 17044.

42 J. Cork, A. K. Whittaker, J. J. Cooper-White and L. Grøndahl, Tensile properties and in vitro degradation of P(TMC-*co*-LLA) elastomers, *J. Mater. Chem. B*, 2015, **3**, 4406.
43 D. G. Sycks, T. Wu, H. S. Park and K. Gall, Tough, stable spiroacetal thiol-ene resin for 3D printing, *J. Appl. Polym. Sci.*, 2018, **135**, 46259.
44 Y. Dou, Z.-P. Wang, W. He, T. Jia, Z. Liu, P. Sun, K. Wen, E. Gao, X. Zhou, X. Hu, J. Li, S. Fang, D. Qian and Z. Liu, Artificial spider silk from ion-doped and twisted core-sheath hydrogel fibres, *Nat. Commun.*, 2019, **10**, 5293.
45 J. L. Yarger, B. R. Cherry and A. van der Vaart, Uncovering the structure–function relationship in spider silk, *Nat. Rev. Mater.*, 2018, **3**, 18008.
46 M. Heim, D. Keerl and T. Scheibel, Spider Silk: From Soluble Protein to Extraordinary Fiber, *Angew. Chem., Int. Ed.*, 2009, **48**, 3584.
47 M. Elices, G. R. Plaza, J. Pérez-Rigueiro and G. V. Guinea, The hidden link between supercontraction and mechanical behavior of spider silks, *J. Mech. Behav. Biomed. Mater.*, 2011, **4**, 658.
48 M. Li, R. Zhang, X. Li, Q. Wu, T. Chen and P. Sun, High-performance recyclable cross-linked polyurethane with orthogonal dynamic bonds: The molecular design, microstructures, and macroscopic properties, *Polymer*, 2018, **148**, 127.
49 Z. Tang, J. Huang, B. Guo, L. Zhang and F. Liu, Bioinspired Engineering of Sacrificial Metal–Ligand Bonds into Elastomers with Supramechanical Performance and Adaptive Recovery, *Macromolecules*, 2016, **49**, 1781.
50 L. Song, T. Zhu, L. Yuan, J. Zhou, Y. Zhang, Z. Wang and C. Tang, Ultra-strong long-chain polyamide elastomers with programmable supramolecular interactions and oriented crystalline microstructures, *Nat. Commun.*, 2019, **10**, 1315.
51 B. Zhang, Z. A. Digby, J. A. Flum, E. M. Foster, J. L. Sparks and D. Konkolewicz, Self-healing, malleable and creep limiting materials using both supramolecular and reversible covalent linkages, *Polym. Chem.*, 2015, **6**, 7368.
52 B. van Minnen, B. Stegenga, M. B. M. van Leeuwen, T. G. van Kooten and R. R. M. Bos, A long-term in vitro biocompatibility study of a biodegradable polyurethane and its degradation products, *J. Biomed. Mater. Res., Part A*, 2006, **76A**, 377.
53 J. Li, X. Feng, B. Liu, Y. Yu, L. Sun, T. Liu, Y. Wang, J. Ding and X. Chen, Polymer materials for prevention of postoperative adhesion, *Acta Biomater.*, 2017, **61**, 21.
54 B. A. van den Beukel, R. de Ree, S. van Leuven, E. A. Bakkum, C. Strik, H. van Goor and R. P. G. ten Broek, Surgical treatment of adhesion-related chronic abdominal and pelvic pain after gynaecological and general surgery: a systematic review and meta-analysis, *Hum. Reprod. Update*, 2017, **23**, 276.
55 T. K. Rajab, M. Wallwiener, C. Planck, C. Brochhausen, B. Kraemer and C. W. Wallwiener, A Direct Comparison of Seprafilm, Adept, Intercoat, and Spraygel for Adhesion Prophylaxis1, *J. Surg. Res.*, 2010, **161**, 246.
56 H. Wang, M. Li, J. Hu, C. Wang, S. Xu and C. C. Han, Multiple Targeted Drugs Carrying Biodegradable Membrane Barrier: Anti-Adhesion, Hemostasis, and Anti-Infection, *Biomacromolecules*, 2013, **14**, 954.